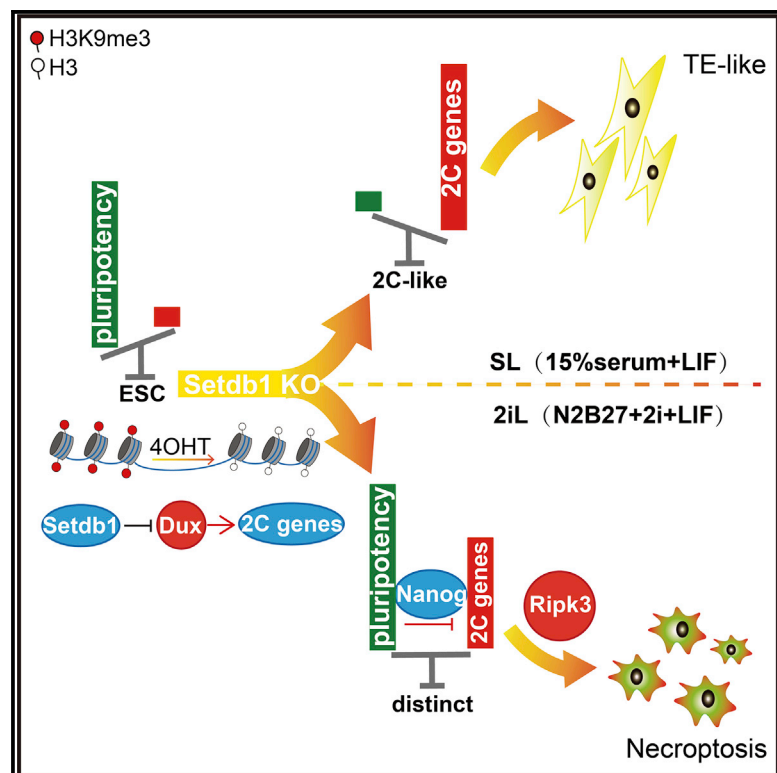


SETDB1-Mediated Cell Fate Transition between 2C-Like and Pluripotent States

Graphical Abstract



Authors

Kaixin Wu, He Liu, Yaofeng Wang, ..., Jie Wang, Duanqing Pei, Jiekai Chen

Correspondence

chen_jiekai@gibh.ac.cn

In Brief

Wu et al. report the essential role of *Setdb1* in the cell fate transition between totipotency and pluripotency. *Setdb1*-KO ESCs activate a group of genes targeted by SETDB1-mediated H3K9 methylation, including *Dux*, then initiate 2C-like totipotency transition. Moreover, *Setdb1*-KO triggers ESC necroptosis in the “ground state” by activating *Ripk3*.

Highlights

- *Setdb1*-KO fails to induce trophectoderm (TE) differentiation in “ground-state” ESCs
- *Setdb1* deficiency initiates 2C-like transition program in a *Dux*-dependent manner
- *Nanog* overexpression suppresses 2C-like transition induced by *Setdb1*-KO
- The “ground-state” *Setdb1*-null ESCs undergo necroptosis by activating *Ripk3*



SETDB1-Mediated Cell Fate Transition between 2C-Like and Pluripotent States

Kaixin Wu,^{1,2,3,4,8} He Liu,^{1,2,3,4,8} Yaofeng Wang,^{4,5} Jiangping He,^{1,2,3,4} Shuyang Xu,^{1,2} Yaping Chen,^{1,2,3} Junqi Kuang,^{1,2,3} Jiadong Liu,^{1,2,3} Lin Guo,^{1,2,4} Dongwei Li,^{1,2,4} Ruona Shi,^{1,2,4} Li Shen,⁶ Yangming Wang,⁷ Xiaofei Zhang,^{1,2,3,4} Jie Wang,^{1,2,4} Duanqing Pei,^{1,2,3,4,5} and Jiekai Chen^{1,2,3,4,9,*}

¹CAS Key Laboratory of Regenerative Biology, Joint School of Life Sciences, Guangzhou Institutes of Biomedicine and Health, Guangzhou Medical University, Chinese Academy of Sciences, Guangzhou, China

²Guangdong Provincial Key Laboratory of Stem Cell and Regenerative Medicine, Guangzhou Institutes of Biomedicine and Health, Chinese Academy of Sciences, Guangzhou 510530, China

³University of Chinese Academy of Sciences, Beijing 100049, China

⁴Guangzhou Regenerative Medicine and Health Guangdong Laboratory (GRMH-GDL), Guangzhou 510005, China

⁵CUHK-GIBH Joint Laboratory of Stem Cell and Regenerative Medicine, Chinese University of Hong Kong, Hong Kong, China

⁶Life Sciences Institute and Stem Cell Institute, Zhejiang University, Hangzhou 310058, China

⁷Beijing Key Laboratory of Cardiometabolic Molecular Medicine, Institute of Molecular Medicine, Peking University, Beijing 100871, China

⁸These authors contributed equally

⁹Lead Contact

*Correspondence: chen_jiekai@gibh.ac.cn

<https://doi.org/10.1016/j.celrep.2019.12.010>

SUMMARY

Known as a histone H3K9 methyltransferase, SETDB1 is essential for embryonic development and pluripotent inner cell mass (ICM) establishment. However, its function in pluripotency regulation remains elusive. In this study, we find that under the “ground state” of pluripotency with two inhibitors (2i) of the MEK and GSK3 pathways, *Setdb1*-knockout fails to induce trophectoderm (TE) differentiation as in serum/LIF (SL), indicating that TE fate restriction is not the direct target of SETDB1. In both conditions, *Setdb1*-knockout activates a group of genes targeted by SETDB1-mediated H3K9 methylation, including *Dux*. Notably, *Dux* is indispensable for the reactivation of 2C-like state genes upon *Setdb1* deficiency, delineating the mechanistic role of SETDB1 in totipotency restriction. Furthermore, *Setdb1*-null ESCs maintain pluripotent marker (e.g., *Nanog*) expression in the 2i condition. This “ground state” *Setdb1*-null population undergoes rapid cell death by activating *Ripk3* and, subsequently, RIPK1/RIPK3-dependent necroptosis. These results reveal the essential role of *Setdb1* between totipotency and pluripotency transition.

INTRODUCTION

The genome senses and integrates intrinsic and environmental signals via epigenetic regulation. This heritable process modulates gene activity through DNA and histone modifications without DNA sequence alteration. Spatiotemporal epigenetic modification plays a crucial role in cell fate decision during embryonic development. As a well-known epigenetic mark of heterochromatin (Stancheva, 2005), histone H3K9 methylation is

crucial to regulate both differentiation and somatic reprogramming (Chen et al., 2013; Liu et al., 2018; Matoba et al., 2014; Nicetto et al., 2019; Soufi et al., 2012; Torrano et al., 2019; Wang et al., 2018; Wei et al., 2017). Among known H3K9 methyltransferases, *Setdb1* is the only molecule whose deficiency leads to peri-implantation lethality (around 3.5–5.5 days post coitum [dpc]) (Dodge et al., 2004), underlying its importance in early embryonic development. SETDB1 was initially identified as an interacting partner of ETS-related transcription factor, ERG (Blackburn et al., 2003; Wang et al., 2003; Yang et al., 2002). *Setdb1*-null blastocysts exhibited defective growth of the inner cell mass (ICM) and the incapability of deriving embryonic stem cell (ESC) lines (Dodge et al., 2004). Besides, SETDB1 may associate with OCT4 to maintain pluripotency of ESC identity and suppress trophectoderm differentiation (Lohmann et al., 2010; Yuan et al., 2009). However, the regulatory mechanism of *Setdb1*-H3K9me during this pluripotency-associated cell fate decision is unclear.

ICM-derived ESCs are pluripotent cells capable of generating various embryonic tissues, except for extraembryonic tissues (Beddington and Robertson, 1989; Tsunoda and McLaren, 1983). In contrast, the cleavage or two-cell (2C) state of embryos retains the totipotency to generate both embryonic and extraembryonic tissues (Beddington and Robertson, 1989; Rodriguez-Terrones et al., 2018; Tsunoda and McLaren, 1983). However, totipotent 2C-like cells arise in extremely low proportion in ESC culture (Macfarlan et al., 2012). At the 2C-like state, endogenous retroviruses (ERVs), particularly MERVL, are transiently repressed (Macfarlan et al., 2012), subsequently reactivating 2C-state marker genes, including members of *Zscan4* and *Usp171* families (Falco et al., 2007; Hendrickson et al., 2017; Hirata et al., 2012; Macfarlan et al., 2012). Meanwhile, core factors of the pluripotency transcriptional network, such as OCT4 and NANOG are degraded in the 2C-like state (Ishiiuchi et al., 2015; Macfarlan et al., 2012), suggesting the incompatibility between pluripotency and totipotency. Notably, the transcription factor *Dux* is a major



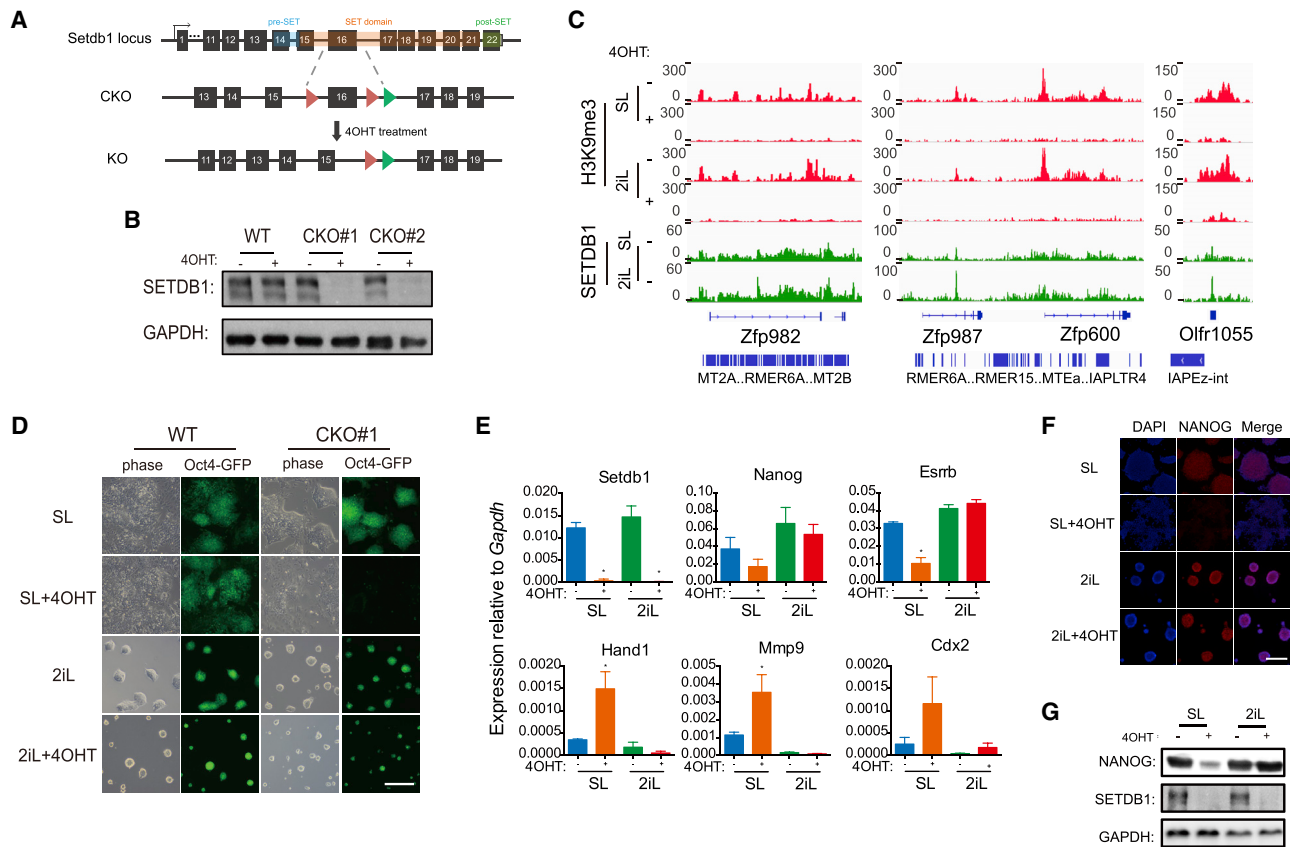


Figure 1. Culturing Conditions Specify Distinct ESC Pluripotency States upon *Setdb1*-KO

(A) *Setdb1*-conditional KO (CKO) strategy via Cre-Lox system. Briefly, two LoxP sites flank exon 16 within SET domain of *Setdb1*. The KO event initiates upon 4OHT addition.

(B) Western blot analysis validated conditional SETDB1 removal in two CKO cell lines at day 3 post 4OHT treatment.

(C) Integrative genomics viewer (IGV) graphs of H3K9me3 occupancy \pm 4OHT treatment, as well as SETDB1 occupancy, in two culturing conditions at *Zfp982*/*Zfp987*, *Zfp600*, and *Olfr1055* loci. Blue lines represent the relative localization of TE.

(D) Phase-contrast and fluorescence microscopic images of wild-type (WT; left panel) and *Setdb1*-CKO (right panel) ESCs cultured in SL/2iL condition with \pm 4OHT treatment. Scale bars, 250 μ m.

(E) qPCR analysis of *Setdb1*, *Nanog*, *Esrrb*, *Hand1*, *Mmp9*, and *Cdx2* in CKO cells \pm 4OHT treatment (n = 3 biological replicates each with 2 technical replicates; error bar, SD; *p < 0.05).

(F) Immunofluorescence (IF) analysis of NANOG in CKO cells \pm 4OHT treatment under two culture conditions. Scale bars, 250 μ m.

(G) Western blot analysis result of samples in (F).

driver inducing zygotic genome activation (ZGA) genes and 2C-like state (De iaco et al., 2017; Eckersley-Maslin et al., 2019; Hendrickson et al., 2017; Whiddon et al., 2017). Additionally, loss of function of *LSD1*, *G9a*, *KAP1*, *SUMO-2*, and *Ring1b* has been reported to facilitate 2C-like state transition from ESCs (Cossec et al., 2018; Hisada et al., 2012; Macfarlan et al., 2011; Maksakova et al., 2013; Rodriguez-Terrones et al., 2018). Although the SETDB1 partner KAP1 is a known restrictor toward the 2C-like state, there is no direct evidence that SETDB1-mediated H3K9me3 inhibits 2C-like state transition.

In this study, we have demonstrated that *Setdb1* deficiency strongly induced 2C-like state marker genes, such as *Zscan4* and *Dux*. However, totipotency transition from *Setdb1*-knockout (KO) ESCs depends on culture conditions. The “ground-state” ESCs cultured with two inhibitors (2i) of MEK1/2 and GSK3 (Ying et al., 2008) underwent rapid cell death during *Setdb1*-

KO-induced 2C-like state transition. Specifically, *Setdb1*-KO-mediated cell death under 2i condition is induced by *Ripk3* upregulation, followed by RIPK1/RIPK3-dependent necroptosis. This chaotic cellular status may attribute to the sustained expression of pluripotency genes. These data revealed that SETDB1-mediated H3K9me3 is essential for pluripotency establishment and pluripotent cell survival, highlighting SETDB1’s role in early embryonic development.

RESULTS

Setdb1-KO in ESCs Does Not Induce Trophectoderm Differentiation under 2i Condition

Previous studies have summarized that SETDB1 is essential for pluripotency maintenance, as *Setdb1* deficiency in the ESCs promotes trophectoderm (TE) differentiation. TE marker genes,

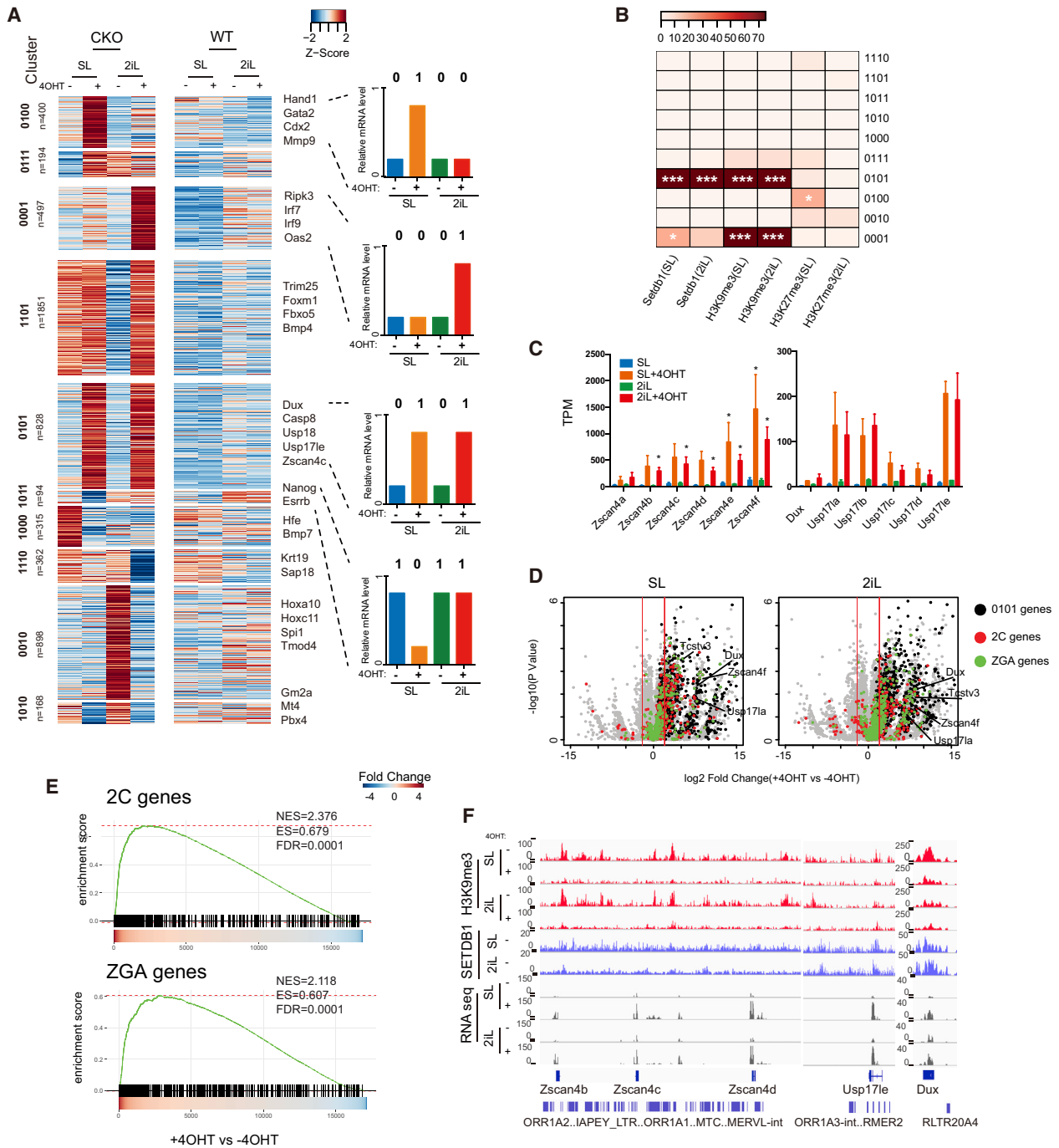


Figure 2. *Setdb1* Deficiency Initiates the Transition into 2C-Like State

(A) Heatmap profile from RNA-seq analysis classifies gene expression of *Setdb1* CKO cells upon SL or 2iL condition into 10 clusters. Simulated mRNA levels of clusters 0100, 0001, 0101, and 1011 are illustrated in the right panel.

(B) A heatmap displays the enrichment of SETDB1 (± 20 kb), H3K9me3 (± 20 kb), and H3K27me3 (± 10 kb) in all clusters that are defined in (A). Significance is derived from a Fisher exact test (* $p < e-30$; *** $p < e-70$).

(C) RNA-seq expression of transcripts per kilobase million (TPM) of 2C-like cell markers in *Setdb1*-CKO cells under both conditions (3 independent RNA-seq experiments; error bar, SD; * $p < 0.05$)

(legend continued on next page)

such as *Cdx2* and *Hand1*, are activated upon *Setdb1* deficiency via conditional KO (CKO) or shRNA knockdown (KD) (Bilodeau et al., 2009; Lohmann et al., 2010; Yuan et al., 2009). However, adjacent genomic regions of these TE marker loci lack H3K9me3 enrichment or credible SETDB1 binding (Figures S1A and S1G), suggesting that SETDB1-mediated H3K9me3 does not directly regulate TE differentiation. Previous reports have demonstrated that the “ground-state” pluripotency of mouse ESC is retained under 2i condition (Ying et al., 2008). To understand the role of SETDB1 during pluripotency regulation, we silenced *Setdb1* using small interfering RNA (siRNA) and cultured ESCs under two conditions: traditional medium supplemented with 15% FBS and LIF (SL), and “ground-state” medium consisting of 2i and LIF (2iL). si*Setdb1* slightly impaired *Oct4*-GFP expression and downregulated pluripotency genes but failed to reactivate TE marker genes in SL (Figures S1A, S1B, and S1D), in contrast to past studies using high-efficiency short hairpin RNA (shRNA) or KO (Li et al., 2017b; Maksakova et al., 2013). After enhancing KD efficiency using two-round siRNA transduction, si*Setdb1* exhibited downregulation of pluripotency genes and reactivation of TE markers in SL (Figures S1C and S1E). Notably, *Setdb1*-KD under 2iL culture failed to resemble the differentiation pattern as in SL (Figures S1B–S1F), demonstrating that *Setdb1* deficiency is not sufficient to suppress pluripotency and induce TE differentiation.

The SET domain of SETDB1 is essential for its H3K9 methyltransferase activity. To identify the regulatory function of SETDB1-mediated H3K9 methylation, we constructed *Setdb1* CKO-ESCs by inserting loxP sites around exon 16, encoding the key part of the SET domain (Figure 1A). Upon tamoxifen treatment, SETDB1 was totally depleted within 3 days in CKO-ESCs consistently expressing CRE-ERT (Figure 1B). Next, we performed H3K9me3/SETDB1 chromatin immunoprecipitation sequencing (ChIP-seq) on CKO-ESCs culturing under both SL and 2iL conditions. The SETDB1-binding and H3K9me3-enrichment patterns are identical between SL and 2iL, and the SETDB1-binding sites highly correlate with H3K9me3 peaks throughout the genome (Figure 1C). Upon depletion of SETDB1 under 3-day tamoxifen treatment, almost all H3K9me3 peaks were wiped out in both SL and 2iL conditions (Figures 1C, S2A, and S2B), indicating *Setdb1* is responsible for the majority of H3K9me3 catalysis throughout the genome, at least in the uniquely mapped regions. We found that *Setdb1*-KO decreased *Oct4*-GFP expression in SL but exhibited no obvious effects in 2iL (Figures 1D, S2C, and S2D). Consistently, *Setdb1*-KO downregulates and upregulates pluripotency genes (i.e., *Nanog* and *Esrrb*) and TE genes (i.e., *Hand1*, *Mmp9*, and *Cdx2*), respectively, in SL (Figure 1E). At the protein level, expression of the pluripotent marker, NANOG, was largely decreased in SL upon *Setdb1*-KO (Figures 1F and 1G). To summarize, *Setdb1* deficiency induced TE differentiation only in SL condition and failed to downregulate pluripotency genes in the ground-state culture

condition. These data indicated that SETDB1 is not responsible for repressing TE markers or safeguarding pluripotency gene expression. Notably, no significant SETDB1-binding or H3K9me3 peaks were observed near TE genes (Figure S1G), suggesting that, contrary to the previous notion, SETDB1 may not directly suppress TE fate.

Setdb1 Deficiency Initiates Totipotent 2C-Like State Transition in ESCs

Next, we performed RNA sequencing (RNA-seq) to investigate the impact of *Setdb1*-KO on the global gene expression in both SL and 2iL conditions (Figure 2A). Differentially expressed genes were categorized into several clusters according to their expression patterns (Figure 2A). We used “0” and “1” to represent the low and high expression levels, respectively. Accordingly, “01” and “10” mark upregulation and downregulation, correspondingly. Cluster 0100 represents genes activated only in SL upon *Setdb1*-KO, including TE development genes such as *Cdx2* and *Hand1* (Figure 2A); cluster 1011 contains pluripotency genes that are suppressed only in SL upon *Setdb1*-KO (Figures 2A and S2E). Of note, these two clusters enrich neither SETDB1 binding nor H3K9me3 occupancy, suggesting that *Setdb1* does not directly regulate these genes (Figure 2B). Cluster 0101, with elevated gene expression upon *Setdb1*-KO in both conditions, enriches both SETDB1 binding and H3K9me3 occupancy (Figure 2B; Table S1). These observations suggested that *Setdb1*-mediated H3K9me3 represses cluster 0101 genes independent of culturing conditions (Figure 2B). Particularly, cluster 0001 genes, which are only upregulated in 2iL upon *Setdb1*-KO, enrich H3K9me3 occupancy in both conditions (Figure 2B). We propose that additional repressive factor other than H3K9me3 suppressed cluster 0001 genes in SL condition. Notably, 0001 cluster has higher DNA methylation level than 0101 clusters (Figure S2H). In addition, it is well known that ground state decreases DNA methylation level greatly (Kumar and Ivanova, 2015). The above evidence suggests that DNA methylation may contribute to the additional inhibitory mechanism. To examine the specificity of SETDB1 regulation, we performed H3K27me3 ChIP-seq and observed that, other than cluster 0100, all *Setdb1*-KO regulated clusters under both conditions are H3K27me3-independent, emphasizing that SETDB1 specifically mediates H3K9me3, directly regulating cluster 0101 genes (Figure 2B). We divided the H3K9me3-occupying regions into two groups: promoter occupation (–1.5/+0.5 kb around transcription start site [TSS]) and others. Specifically, we found that 0101/0001 clusters enriched H3K9me3 particularly at the promoter region (Figure S2I). Moreover, promoter-occupied H3K9me3 is critical for repression of its nearby genes (Figure S2J).

We further investigated the identified SETDB1-regulating genes. We identified known 2C-like cell markers such as *Zscan4* and *Usp17l* in the cluster 0101 and validated with RT-qPCR (Figures 2A, 2C, 2D, S2F, and S2G), suggesting *Setdb1* deficiency induces the 2C-specific program. Comparing RNA-seq data with

(D) Volcano plots showing the fold changes transcriptomes of *Setdb1*-CKO cells in SL/2iL. Significance is derived from t test. Black, red, and green dots represent 0101, 2C, and ZGA genes, correspondingly.

(E) Gene set enrichment analysis (GSEA) illustrating the enrichment of 2C and ZGA gene sets among upregulated genes upon loss of *Setdb1*.

(F) IGV graphs illustrate H3K9me3 occupancy \pm 4OHT treatment, SETDB1 occupancy, together with transcriptomic expression in two culturing conditions at selected 2C-gene marker loci.

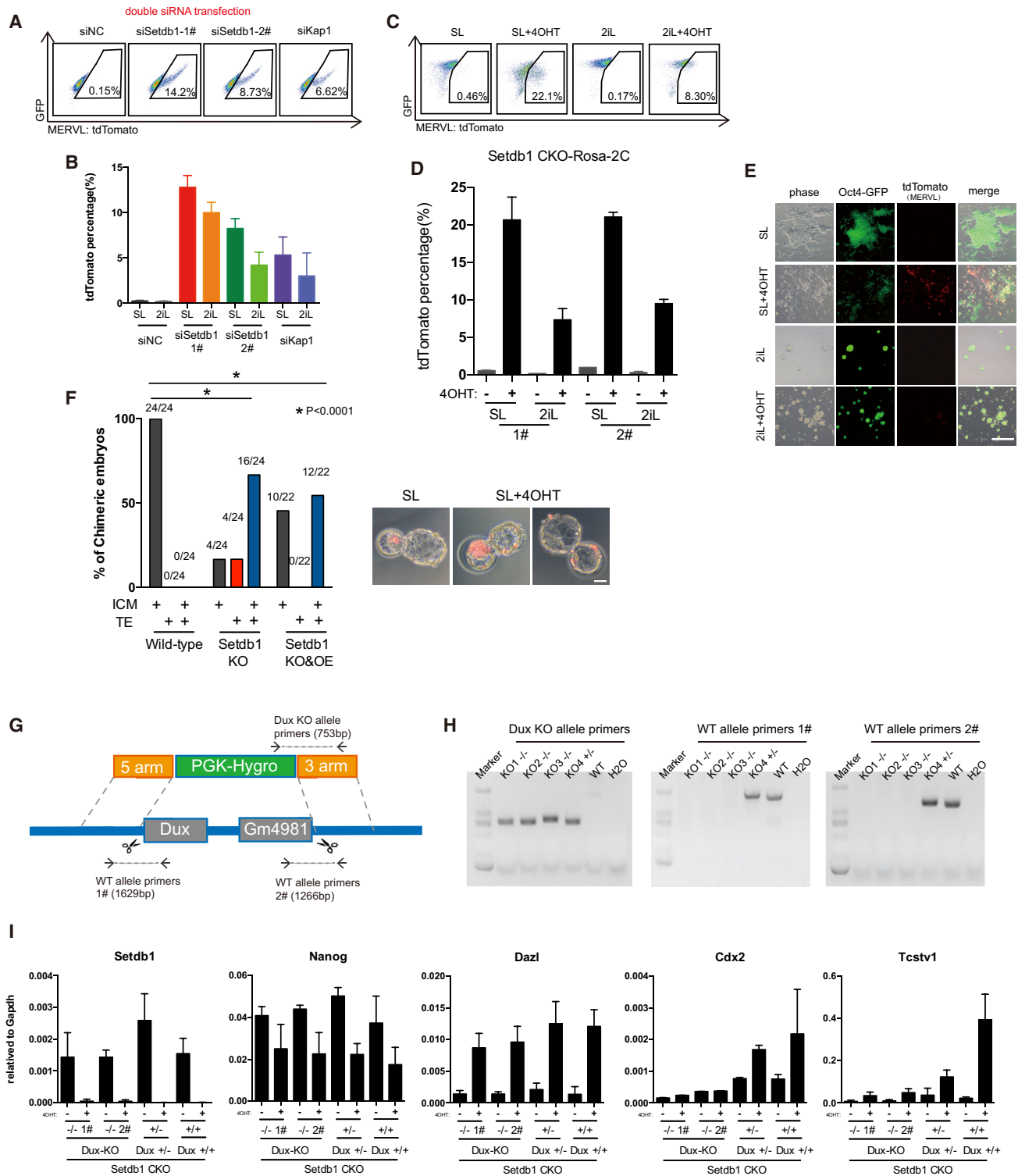


Figure 3. *Setdb1* Deficiency Activates MERVL and Contributes to the Generation of Embryonic and Extraembryonic Tissues in a *Dux*-Dependent Manner

(A) Flow cytometry analysis showing MERVL::tdTomato (x axis) and OCT4-GFP (y axis) expression following siRNA knockdown (KD) of *Setdb1* and *Kap1* via double siRNA transfection.

(B) The column graph summarizes the percentages of cells with MERVL::tdTomato level following *Setdb1* and *Kap1*-KD in SL/2iL condition (n = 3; error bar, SEM).

(C) Flow cytometry analysis illustrating *Rosa26*-targeted MERVL::tdTomato (x axis) and OCT4-GFP (y axis) expression upon *Setdb1*-CKO in SL and 2iL.

(legend continued on next page)

pre-defined 2C and ZGA gene sets (Li et al., 2017b; Macfarlan et al., 2012), we observed significant enrichment of 2C/ZGA genes in the upregulated population upon *Setdb1*-KO (Figures 2D and 2E). ESCs are known to derive a limited fraction of 2C-like cells highly expressing *Zscan4* family, *Dux*, and MERVL (Falco et al., 2007; Hendrickson et al., 2017; Hirata et al., 2012; Macfarlan et al., 2012). We observed that SETDB1 binding and H3K9me3 were enriched nearby some 2C-like state genes such as *Dux* and *Zscan4* in a SETDB1-dependent fashion (Figure 2F), suggesting that SETDB1-mediated H3K9me3 hindered 2C-like state transition in the wild-type ESCs. Of note, SETDB1-mediated 2C-like and TE gene regulation was highly dose sensitive, as increased TE markers and 2C markers were only observed upon *Setdb1*-CKO and high-efficiency KD (Figures S1B–S1E, S3A, and S3B). Furthermore, we repurposed the reported RNA-seq data upon *Setdb1*-KO (Karimi et al., 2011) and validated the upregulation of 2C-like state genes and MERVL (Figures S3C and S3D). These results supported the notion that *Setdb1*-KO or high-efficiency KD reactivated 2C-like-state genes.

We then knocked down *Setdb1* in a MERVL::tdTomato reporter ESC line as an indicator of 2C-like state. Only high-efficiency *Setdb1* KD with two-round siRNA transfection induced tdTomato-positive cells (Figures 3A, 3B, S3E, and S3F). Furthermore, we generated Rosa26-targeted MERVL::tdTomato knockin lines on *Setdb1*-CKO ESCs and observed a similar phenotype of the si*Setdb1* system (Figures 3C–3E). In detail, *Setdb1*-KO exhibited up to 22% of tdTomato-positive cells, comparing to 14.2% in si*Setdb1*. Besides, 2iL condition partially dampened tdTomato-positive rate comparing to SL upon *Setdb1*-KD or KO (Figures 3B and 3D). To define the cell fate potential of *Setdb1*-KO ESCs in the embryonic development, we aggregated *Setdb1*-KO ESCs with 8-cell embryos. *Setdb1*-KO ESCs exhibited high incorporation frequency (16/24) into both ICM and TE, while wild-type ESCs were incapable of TE incorporation (Figure 3F). This *Setdb1*-KO-specific TE-incorporation is complemented by *Setdb1*-OE, as incorporation of *Setdb1*-KO cells were decreased in the TE layer of the chimeric embryo. Together, these observations validated that *Setdb1*-KO facilitates transition into the totipotent “2C-like state.”

2C-Like State Transition Induced by *Setdb1*-KO Is *Dux* Dependent and Suppressed by *Nanog* Overexpression

Free of H3K9 methylation occupation, MERVL elements are known to be regulated by *Dux*, a critical initiator of 2C-like state transition from ESCs (Cossec et al., 2018; Maksakova et al., 2013; Percharde et al., 2018). As SETDB1 directly regulates

Dux loci (Figure 2F), we constructed *Dux*-KO *Setdb1* CKO ESCs to measure the contribution of *Dux* during SETDB1-mediated 2C-like transition (Figures 3G and 3H). We found that *Dux*-KO eliminated *Setdb1*-KO-induced 2C-like genes and TE genes activation, while it did not affect *Nanog* decrease and imprinted genes activation (i.e., *Dazl*, *Mmp12*) (Figures 3I and S3G), demonstrating that *Dux* plays a dominant role in 2C-like induction upon *Setdb1*-KO.

Degradation of pluripotency proteins such as NANOG/OCT4 is a known property of 2C-like transition from ESCs (Ishiyuchi et al., 2015; Macfarlan et al., 2012). However, we observed that *Setdb1*-KO cells in 2iL retain NANOG expression (Figure 1F). Even though *Dux* showed a dominant role in 2C-like program initiation (Figures 3G–3I), we wonder whether pluripotency exit is required for 2C-like transition. We overexpressed *Nanog*/Oct4 in *Setdb1*-CKO ESCs (CKO-*Nanog*) and found that CKO-*Nanog* cells failed to activate 2C-like program (Figures 4A, 4B, and S4A). These observations demonstrated that pluripotency transcription network impairs 2C-like program, echoing that 2iL inhibits transition from pluripotent to 2C-like state.

Setdb1-KO Induces Necroptosis in 2iL Condition

The 2iL condition restored the pluripotent network after *Setdb1*-KO (Figures 1F, 1G, and S2E). However, we found that these Oct4-GFP⁺/*Nanog*⁺ ESCs were not able to passage, suggesting initiation of programs preventing cell proliferation (Figure 5A). Among the 0001 genes, we identified genes relative to programmed cell death and immune response such as *Ripk3*, *Oas2*, and *Irf7* (Figures 2A and 5B). RT-qPCR validated their reactivation in *Setdb1*-KO ESCs under 2iL (Figure 5B). In addition, cluster 0101 gene *Caspase 8* (*Casp8*) was derepressed upon *Setdb1*-KO (Figures 2A, S5A), suggesting that programmed cell death may serve as the pathway to prevent *Setdb1*^{-/-} ESC proliferation in 2iL condition. Moreover, the upstream (5') of *Ripk3* is marked with *Setdb1*-dependent H3K9me3, centering on an IAPLTR2 element with lower DNA methylation upon 2iL (Figure S5B), suggesting double repressive mechanism for cluster 0001 genes. Then we tested small-molecule compounds targeting apoptosis (Z-VAD) (Fearhead et al., 1995; Slee et al., 1996) and necroptosis (Nec-1) (Degterev et al., 2005). Nec-1, but not Z-VAD, reversed the proliferation blockage effect of *Setdb1*-KO (Figures 5C, 5D, and S5C). Nec-1 is known as an inhibitor for RIPK1 phosphorylation and activation, suggesting RIPK1-dependent programmed necroptosis is induced by *Setdb1* KO in 2iL condition.

(D) A column graph summarizes the percentages of cells with Rosa26-targeted MERVL::tdTomato level upon *Setdb1*-KO in SL/2iL condition (n = 3; error bar, SEM).

(E) Phase-contrast and fluorescence microscopic images of *Setdb1* KO in Rosa26-targeted MERVL-TdTomato reporter cell line under SL/2iL condition. Scale bars, 250 μ m.

(F) A column graph on the left panel illustrates the percentage of chimeric embryos after injecting WT, *Setdb1*-KO, and the *Setdb1*-OE rescued ESCs (the p value was determined by Fisher's exact test, *p < 0.0001). The right panel displays the fluorescence microscopic images of 8-cell embryo injected with mCherry-positive *Setdb1*-CKO ESCs. Scale bars, 20 μ m.

(G) Schematic view of the *Dux* KO strategy. Arrows indicate primer locations.

(H) An agarose gel image illustrating the PCR-based genotyping assay of the *Dux*-KO ESCs. Genotyping results of 4 ESCs are shown. *Dux*-KO1, KO2, and KO3 are double KO cell lines, whereas *Dux*-KO4 is a single KO cell line.

(I) qPCR analysis demonstrating the expression of *Setdb1*, *Nanog*, the mprinted gene, *Dazl*, the trophectoderm gene, *Cdx2*, and the 2C gene *Tcstv1* in *Setdb1*-CKO after *Dux* KO (n = 2, each with 2 technical replicates; error bar, SD).

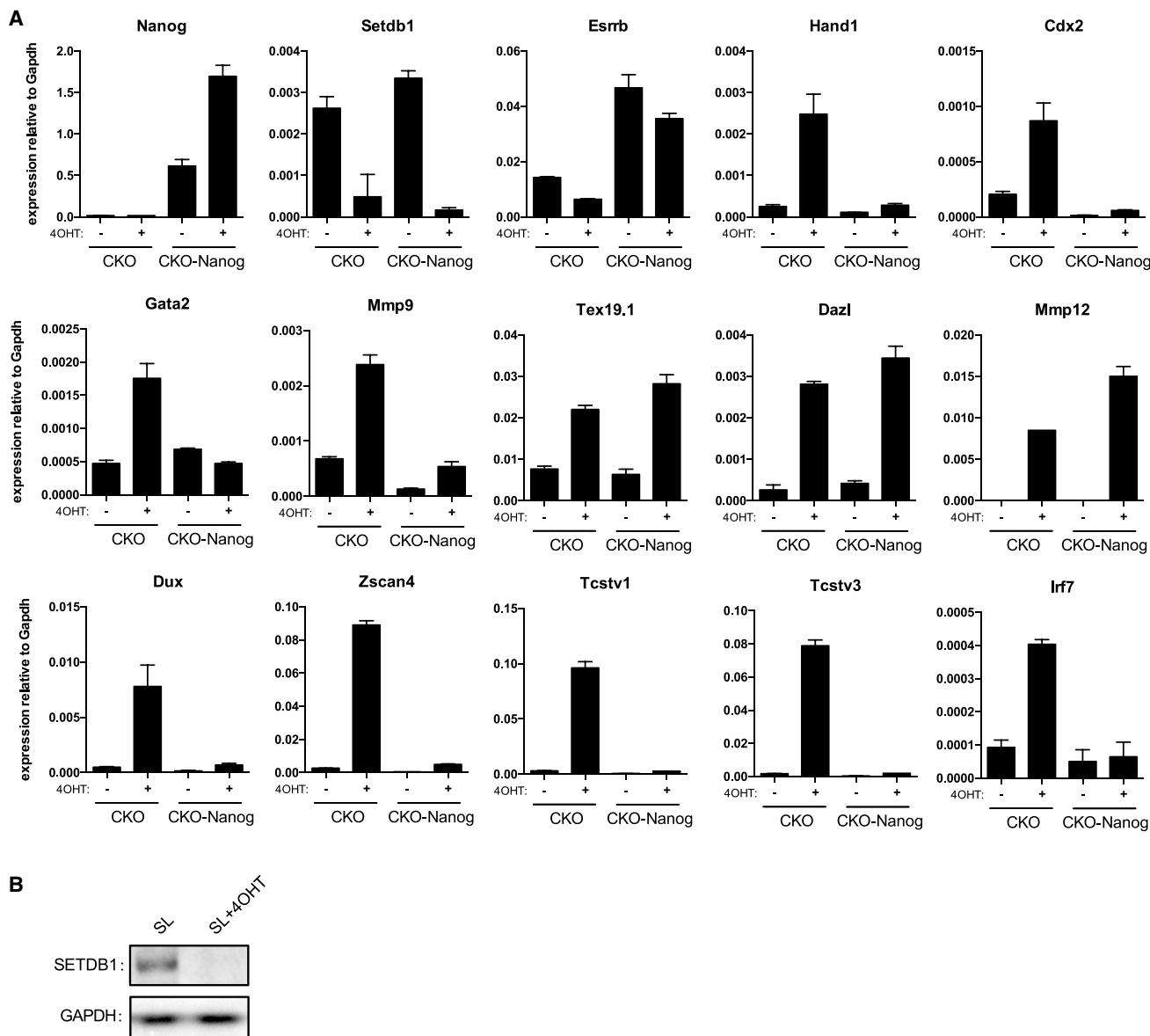


Figure 4. *Nanog*-OE Inhibits the Induction of 2C-like Program upon *Setdb1* Deficiency

(A) qPCR analysis the expression of *Setdb1*, *Nanog*, *Esrrb*, trophectoderm genes (i.e., *Hand1*, *Mmp9*, *Cdx2*, *Gata2*), 2C genes (i.e., *Dux*, *Zscan4*, *Tcstv1*, *Tcstv3*), imprinted genes (i.e., *Dazl*, *Mmp12*, *Tex19.1*), and *Irf7* in CKO cells under SL ± 4OHT treatment upon *Nanog* overexpression (OE) (n = 3, each with 2 technical replicates; error bar, SD).

(B) Western blot analysis demonstrates the expression of SETDB1 in *Setdb1*-KO ESCs upon *Nanog*-OE.

We then performed immunoprecipitation-mass spectrometry (IP-MS) of RIPK1 before and after *Setdb1*-KO in 2iL condition (Figure 5E; Table S2). As reported, RIPK1 constitutively interacted with FADD (Lu et al., 2011; Shan et al., 2018), while it only interacted with RIPK3 upon *Setdb1*-KO (Figures 5E and 5F). As necrosome assembly is a known process depending on RIPK1-RIPK3 interaction (Cho et al., 2009; Shan et al., 2018; Wegner et al., 2017), these results indicated that *Setdb1*-KO triggered necrosome formation. Consistently, phospho-RIPK1 and phospho-MLKL were detected by western blotting in *Setdb1*-KO ESCs culturing in 2iL (Figure 5G). RIPK1 and

MLKL were also slightly phosphorylated in SL condition (Figure 5G), consistent with the previous observation that Nec-1 mildly promoted the viability of *Setdb1*-KO cells in SL condition (Figures 5D and S5C). As *Ripk3* is activated by *Setdb1* deficiency in 2iL condition at the mRNA (Figures 2A and 5B) and protein level (Figure 5G), we examined the impact of *Ripk3* activation on *Setdb1*-KO-induced programmed necrosis. Two independent *Ripk3* shRNAs, but not *Casp8* shRNA, rescued the cell viability loss upon *Setdb1* deficiency (Figures 5H, 5I, and S5D). These results indicated *Setdb1*-KO induce necroptosis in 2iL through activating *Ripk3*.

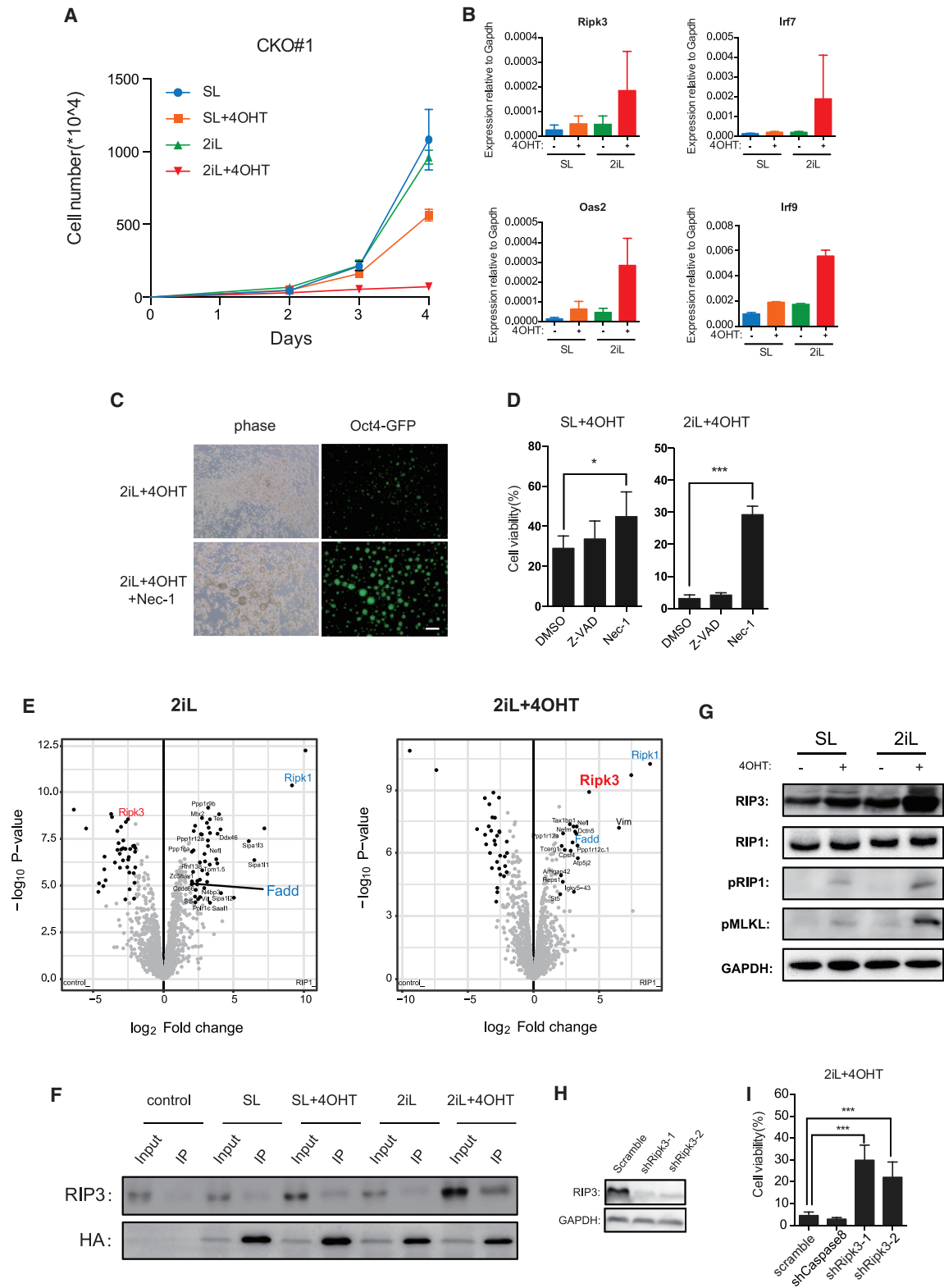


Figure 5. *Setdb1*-KO Induces Necroptosis in 2iL Condition by Activating *Ripk3*

(A) Cell proliferation assay was performed on CKO cells under SL/2iL from day 0 to day 4 (n = 2; error bar, SD).

(B) qPCR analysis of *Ripk3*, *Oas2*, *Irf7*, and *Irf9* gene expression in CKO cells with/without 4OHT treatment (n = 3, each with 2 technical replicates; error bar, SD).

(legend continued on next page)

DISCUSSION

In this study, we conditionally depleted *Setdb1* in SL or 2iL conditions and demonstrated that SETDB1-mediated H3K9me3 is responsible for the suppression of 2C-like state genes. Specifically, activation of *Dux* is essential for *Setdb1*-KO-induced 2C-like program. Meanwhile, TE genes were reactivated only in SL condition and lack of either *Setdb1* binding or H3K9me3 occupancy. Distinct from the pluripotency, the 2C-like state acquired totipotency with the potential of deriving trophectoderm fate (Beddington and Robertson, 1989; Rodriguez-Terrones et al., 2018; Tsunoda and McLaren, 1983). Although there may be other essential factors, we showed that *Dux*-KO ESCs failed to activate TE genes upon *Setdb1* KO (Figures 3I and S3G), indicating 2C-like transition is required for TE activation in SL condition. Therefore, we propose that the *Setdb1*-KO promoted TE differentiation depends on the induction of 2C-like state, thus, a secondary effect of *Setdb1* deficiency.

Although *Setdb1* deficiency is acquiescently correspondent to 2C-like transition, there is no substantial evidence. Instead, two previous studies claimed that *Setdb1*-KD hardly activated MERVL elements, the 2C-specific genes (Li et al., 2017b; Maksakova et al., 2013). As our study observed that 2C-like transition induced by *Setdb1* deficiency is a dose-sensitive event (Figures 3A–3D; Table S3), we proposed that residual SETDB1 in Li's and Maksakova's system impeded MERVL activation. Our data confirmed that regular siRNA/shRNA KD of *Setdb1* hardly activates MERVL reporter and 2C-like genes (Figures S3A–S3C). Echoing that the ground state blocks 2C-like transition, we observed that 2iL inhibited more than 50% MERVL::TdTomato expression upon *Setdb1*-CKO (Figure 3D) (Macfarlan et al., 2012). Consistently, pluripotency factors such as *Nanog/Oct4* prevented 2C gene activation and TE differentiation (Figures 4A and S4A), supporting that pluripotent state precedes the establishment of 2C-like transition (Fu et al., 2019; Rodriguez-Terrones et al., 2018). It is intriguing that 2C-like cells in 2iL expressed both pluripotency and totipotency markers, resulting in a distinct stage apart from the SL-induced 2C-like totipotency (Figures S5E–S5G). Toward necroptosis or totipotency, the cell fate following pluripotency state in 2iL remains to be determined.

Recent work manifested the unexpected minimal impact of *Dux* on ZGA (Chen and Zhang, 2019). Notably, most *Dux* targets in 2C-like cells are regularly activated in maternal and zygotic KO embryos. They attributed the observation to the divergence of 2C-like regulation between 2-cell embryos and ESCs. Indeed, any ESC studies have demonstrated that *Dux* is required to activate the 2C program under *Dppa2/4* OE, *Ubc9* KO, *Kap1* KO, and LINE1 KD conditions (Cossec et al., 2018; Eckersley-Maslin et al., 2019; Percharde et al., 2018; Rodriguez-Terrones et al.,

2018; Yan et al., 2019). Our study revealed that *Setdb1*-KO-induced activation of 2C program is highly dependent on *Dux* (Figures 3G–3I and S3G), elucidating the indisputable role of *Dux* in 2C-like program activation.

Along with *Kap1*, *Setdb1* is responsible for ERV silencing (Collins et al., 2015; Kato et al., 2018; Liu et al., 2014; Matsui et al., 2010; Sharif et al., 2016). Similarly, we observed that the majority of *Setdb1*-dependent H3K9me3 peaks reside at transposon elements or long terminal repeat (data not shown; Jordan et al., 2003). Notably, an IAPLTR2 element has been found upstream of *Ripk3*, marked with *Setdb1*-dependent H3K9me3 and lower DNA methylation upon 2iL (Figure S5B). As both H3K9me3 and DNA methylation are known to regulate IAP element, the differential regulation of *Ripk3* upon two culturing conditions is possibly due to these dual epigenetic modulation (Deniz et al., 2018).

Mice lacking either *Ripk3* or *Mkl1*, the core necroptotic regulators, are able to survive adulthood (Li et al., 2017a), understating the regulatory role of necroptosis during development. Here, we revealed *Setdb1* depletion in 2iL initiates necroptosis via RIPK3, followed by RIPK1/3-induced necrosome assembly. Caspase 8 (CASP8), the necroptotic suppressor, exhibited accumulation of its pro-active form in the *Setdb1*-KO sample under 2iL condition, but not sufficient to block necroptosis (Figure S5H; Weinlich et al., 2017). Moreover, *Nec-1* suppressed necroptosis upon *Setdb1*-KO independent of *Dux* (Figure S5I), suggesting that 2C-like transition is dispensable for *Setdb1*-KO-induced necroptosis in 2iL. The underlying mechanism of necroptotic transition from pluripotency state requires further investigation.

To conclude, our study elucidated the restriction role of SETDB1-mediated H3K9 methylation during pluripotency to totipotency transition, especially, through epigenetic silencing of ERV loci and relevant genes such as *Dux*. Consequently, *Setdb1* deficiency causes defect of ICM generation in embryonic development and undergoes 2C-like state transition in pluripotent stem cells. Investigation toward SETDB1-centered epigenetic regulation provides mechanistic insights of cell fate transition and highlights potential therapeutic targets during early embryonic developmental defects.

STAR★METHODS

Detailed methods are provided in the online version of this paper and include the following:

- KEY RESOURCES TABLE
- LEAD CONTACT AND MATERIALS AVAILABILITY
- EXPERIMENTAL MODEL AND SUBJECT DETAILS
 - Mouse Strains
 - Cell Lines and Cell Culture Condition

(C) Phase-contrast and fluorescence microscopic images of *Nec-1* rescues cell death induced by *Setdb1* KO in 2iL condition. Scale bars, 250 μ m.

(D) Cell viability assay of DMSO, Z-VAD, and *Nec-1*-treated *Setdb1*-KO using CCK8 test (n = 3 independent experiments; error bar, SEM; *p < 0.05 and ***p < 0.001).

(E) Volcano plots showing the RIPK1-hemagglutinin (HA) interactome of *Setdb1*-CKO cells in 2iL generated from HA-IP-MS analysis (n = 3).

(F) Coimmunoprecipitation (IP) assay demonstrating the interaction between HA-tagged *Ripk1* and *Ripk3* in CKO cell cultured in SL/2iL and \pm 4OHT treatment.

(G) Western blot analysis of the necroptotic markers such as p-RIP1 and p-MLKL in CKO cell cultured in SL/2iL and \pm 4OHT treatment.

(H) Western blot analysis to verify the efficiency of the two shRNAs targeting *Ripk3*.

(I) The percentage of cell viability upon shRNA treatment after *Setdb1* KO (n = 3; error bar, SD; ***p < 0.001).

● **METHOD DETAILS**

- Generation of Setdb1 Conditional Knockout OG2 mES Cell
- Construction of Reporter Cell Lines
- Gene Knockdown Assay
- Western Blot
- Immunofluorescence Staining
- Cell Survival Assay
- Flow Cytometry
- Co-immunoprecipitation (Co-IP)
- Immunoprecipitation (IP)-MS
- Mass Spectrometry Analysis
- Native ChIP
- ChIP-Seq
- qRT-PCR and RNA-Seq
- RNA-Seq, ChIP-Seq Analysis

● **QUANTIFICATION AND STATISTICAL ANALYSIS**

● **DATA AND CODE AVAILABILITY**

- Accession Numbers

SUPPLEMENTAL INFORMATION

Supplemental Information can be found online at <https://doi.org/10.1016/j.celrep.2019.12.010>.

ACKNOWLEDGMENTS

We thank Shangtao Cao, Shilong Shu, Wei Pang, and Qiongzi Quan for experimental assistance. We appreciate Prof. Yue Huang for sharing MERVL reporter knockin plasmid. We thank the Guangzhou Branch of the Supercomputing Center of Chinese Academy of Sciences for its support. This work was supported by the National Key R&D Program of China (2019YFA0110200 and 2016YFA0100400), the Key Research and Development Program of Guangzhou Regenerative Medicine and Health Guangdong Laboratory (2018GZR110104003), the Science and Technology Program of Guangzhou (201804020052), the National Natural Science Foundation of China (31771424 and 31401084), and the Frontier Science Research Program of the CAS (ZDBS-LY-SM007).

AUTHOR CONTRIBUTIONS

K.W. and H.L. performed the major experiments. Y.W., J.H., S.X., and J.W. performed the bioinformatics analysis. K.W. performed the ChIP, colIP, and western blotting experiments. K.W. and H.L. performed cell culture experiments, and H.L. performed RNA-seq experiments. Y.C., J.K., J.L., L.G., and D.L. contributed to the work, and R.S. performed IP-MS. K.W., J.W., and J.C. wrote the manuscript. Y.W., L.S., X.Z., and D.P. helped to improve it. J.C. conceived and supervised the entire study.

DECLARATION OF INTERESTS

The authors declare no competing interests.

Received: May 13, 2019
 Revised: September 29, 2019
 Accepted: December 3, 2019
 Published: January 7, 2020

REFERENCES

Beddington, R.S., and Robertson, E.J. (1989). An assessment of the developmental potential of embryonic stem cells in the midgestation mouse embryo. *Development* *105*, 733–737.

Bilodeau, S., Kagey, M.H., Frampton, G.M., Rahl, P.B., and Young, R.A. (2009). SetDB1 contributes to repression of genes encoding developmental regulators and maintenance of ES cell state. *Genes Dev.* *23*, 2484–2489.

Blackburn, M.L., Chansky, H.A., Zielinska-Kwiatkowska, A., Matsui, Y., and Yang, L. (2003). Genomic structure and expression of the mouse ESET gene encoding an ERG-associated histone methyltransferase with a SET domain. *Biochim. Biophys. Acta* *1629*, 8–14.

Castro-Diaz, N., Ecco, G., Coluccio, A., Kapopoulou, A., Yazdanpanah, B., Friedli, M., Duc, J., Jang, S.M., Turelli, P., and Trono, D. (2014). Evolutionally dynamic L1 regulation in embryonic stem cells. *Genes Dev.* *28*, 1397–1409.

Chen, Z., and Zhang, Y. (2019). Loss of DUX causes minor defects in zygotic genome activation and is compatible with mouse development. *Nat. Genet.* *51*, 947–951.

Chen, J., Liu, H., Liu, J., Qi, J., Wei, B., Yang, J., Liang, H., Chen, Y., Chen, J., Wu, Y., et al. (2013). H3K9 methylation is a barrier during somatic cell reprogramming into iPSCs. *Nat. Genet.* *45*, 34–42.

Cho, Y.S., Challa, S., Moquin, D., Genga, R., Ray, T.D., Guildford, M., and Chan, F.K. (2009). Phosphorylation-driven assembly of the RIP1-RIP3 complex regulates programmed necrosis and virus-induced inflammation. *Cell* *137*, 1112–1123.

Collier, A.J., Panula, S.P., Schell, J.P., Chovanec, P., Plaza Reyes, A., Petropoulos, S., Corcoran, A.E., Walker, R., Douagi, I., Lanner, F., et al. (2017). Comprehensive Cell Surface Protein Profiling Identifies Specific Markers of Human Naive and Primed Pluripotent States. *Cell Stem Cell* *20*, 874–890 e877.

Collins, P.L., Kyle, K.E., Egawa, T., Shinkai, Y., and Oltz, E.M. (2015). The histone methyltransferase SETDB1 represses endogenous and exogenous retroviruses in B lymphocytes. *Proc. Natl. Acad. Sci. USA* *112*, 8367–8372.

Cossec, J.C., Theurillat, I., Chica, C., Bua Aguin, S., Gaume, X., Andrieux, A., Iturbide, A., Jouvion, G., Li, H., Bossis, G., et al. (2018). SUMO Safeguards Somatic and Pluripotent Cell Identities by Enforcing Distinct Chromatin States. *Cell Stem Cell* *23*, 742–757.e8.

De Iaco, A., Planet, E., Coluccio, A., Verp, S., Duc, J., and Trono, D. (2017). DUX-family transcription factors regulate zygotic genome activation in placental mammals. *Nat. Genet.* *49*, 941–945.

Degterev, A., Huang, Z., Boyce, M., Li, Y., Jagtap, P., Mizushima, N., Cuny, G.D., Mitchison, T.J., Moskowitz, M.A., and Yuan, J. (2005). Chemical inhibitor of nonapoptotic cell death with therapeutic potential for ischemic brain injury. *Nat. Chem. Biol.* *1*, 112–119.

Deniz, Ö., de la Rica, L., Cheng, K.C.L., Spensberger, D., and Branco, M.R. (2018). SETDB1 prevents TET2-dependent activation of IAP retroelements in naïve embryonic stem cells. *Genome Biol.* *19*, 6.

Dodge, J.E., Kang, Y.K., Beppu, H., Lei, H., and Li, E. (2004). Histone H3-K9 methyltransferase ESET is essential for early development. *Mol. Cell Biol.* *24*, 2478–2486.

Eckersley-Maslin, M., Alda-Catalinas, C., Blotenburg, M., Kreibich, E., Krueger, C., and Reik, W. (2019). Dppa2 and Dppa4 directly regulate the Dux-driven zygotic transcriptional program. *Genes Dev.* *33*, 194–208.

Falco, G., Lee, S.L., Stanghellini, I., Bassey, U.C., Hamatani, T., and Ko, M.S. (2007). Zscan4: a novel gene expressed exclusively in late 2-cell embryos and embryonic stem cells. *Dev. Biol.* *307*, 539–550.

Fearnhead, H.O., Dinsdale, D., and Cohen, G.M. (1995). An interleukin-1 beta-converting enzyme-like protease is a common mediator of apoptosis in thymocytes. *FEBS Lett.* *375*, 283–288.

Fu, X., Wu, X., Djekidel, M.N., and Zhang, Y. (2019). Myc and Dnmt1 impede the pluripotent to totipotent state transition in embryonic stem cells. *Nat. Cell Biol.* *21*, 835–844.

Habibi, E., Brinkman, A.B., Arand, J., Kroeze, L.I., Kerstens, H.H., Matarese, F., Lepikhov, K., Gut, M., Brun-Heath, I., Hubner, N.C., et al. (2013). Whole-genome bisulfite sequencing of two distinct interconvertible DNA methylomes of mouse embryonic stem cells. *Cell Stem Cell* *13*, 360–369.

Hasson, D., Panchenko, T., Salimian, K.J., Salman, M.U., Sekulic, N., Alonso, A., Warburton, P.E., and Black, B.E. (2013). The octamer is the major form of

- CENP-A nucleosomes at human centromeres. *Nat. Struct. Mol. Biol.* **20**, 687–695.
- Heinz, S., Benner, C., Spann, N., Bertolino, E., Lin, Y.C., Laslo, P., Cheng, J.X., Murre, C., Singh, H., and Glass, C.K. (2010). Simple combinations of lineage-determining transcription factors prime cis-regulatory elements required for macrophage and B cell identities. *Mol. Cell* **38**, 576–589.
- Hendrickson, P.G., Doráis, J.A., Grow, E.J., Whiddon, J.L., Lim, J.W., Wike, C.L., Weaver, B.D., Pflueger, C., Emery, B.R., Wilcox, A.L., et al. (2017). Conserved roles of mouse DUX and human DUX4 in activating cleavage-stage genes and MERVL/HERVL retrotransposons. *Nat. Genet.* **49**, 925–934.
- Hirata, T., Amano, T., Nakatake, Y., Amano, M., Piao, Y., Hoang, H.G., and Ko, M.S. (2012). Zscan4 transiently reactivates early embryonic genes during the generation of induced pluripotent stem cells. *Sci. Rep.* **2**, 208.
- Hisada, K., Sánchez, C., Endo, T.A., Endoh, M., Román-Trufero, M., Sharif, J., Koseki, H., and Vidal, M. (2012). RYBP represses endogenous retroviruses and preimplantation- and germ line-specific genes in mouse embryonic stem cells. *Mol. Cell Biol.* **32**, 1139–1149.
- Hunter, J.D. (2007). Matplotlib: A 2D graphics environment. *Computing in Science and Engineering* **9**, 90–95.
- Ishiyuchi, T., Enriquez-Gasca, R., Mizutani, E., Bošković, A., Ziegler-Birling, C., Rodríguez-Terrones, D., Wakayama, T., Vaquerizas, J.M., and Torres-Padilla, M.E. (2015). Early embryonic-like cells are induced by downregulating replication-dependent chromatin assembly. *Nat. Struct. Mol. Biol.* **22**, 662–671.
- Jordan, I.K., Rogozin, I.B., Glazko, G.V., and Koonin, E.V. (2003). Origin of a substantial fraction of human regulatory sequences from transposable elements. *Trends Genet.* **19**, 68–72.
- Karimi, M.M., Goyal, P., Maksakova, I.A., Bilenky, M., Leung, D., Tang, J.X., Shinkai, Y., Mager, D.L., Jones, S., Hirst, M., and Lorincz, M.C. (2011). DNA methylation and SETDB1/H3K9me3 regulate predominantly distinct sets of genes, retroelements, and chimeric transcripts in mESCs. *Cell Stem Cell* **8**, 676–687.
- Kato, M., Takemoto, K., and Shinkai, Y. (2018). A somatic role for the histone methyltransferase Setdb1 in endogenous retrovirus silencing. *Nat. Commun.* **9**, 1683.
- Kumar, I., and Ivanova, N. (2015). Moving Toward the Ground State. *Cell Stem Cell* **17**, 375–376.
- Kumar, V., Muratani, M., Rayan, N.A., Kraus, P., Lufkin, T., Ng, H.H., and Prabhakar, S. (2013). Uniform, optimal signal processing of mapped deep-sequencing data. *Nat. Biotechnol.* **31**, 615–622.
- Langmead, B., and Salzberg, S.L. (2012). Fast gapped-read alignment with Bowtie 2. *Nat. Methods* **9**, 357–359.
- Li, D., Meng, L., Xu, T., Su, Y., Liu, X., Zhang, Z., and Wang, X. (2017a). RIPK1-RIPK3-MLKL-dependent necrosis promotes the aging of mouse male reproductive system. *eLife* **6**, e27692.
- Li, P., Wang, L., Bennett, B.D., Wang, J., Li, J., Qin, Y., Takaku, M., Wade, P.A., Wong, J., and Hu, G. (2017b). Rif1 promotes a repressive chromatin state to safeguard against endogenous retrovirus activation. *Nucleic Acids Res.* **45**, 12723–12738.
- Liu, S., Brind'Amour, J., Karimi, M.M., Shirane, K., Bogutz, A., Lefebvre, L., Sasaki, H., Shinkai, Y., and Lorincz, M.C. (2014). Setdb1 is required for germline development and silencing of H3K9me3-marked endogenous retroviruses in primordial germ cells. *Genes Dev.* **28**, 2041–2055.
- Liu, X., Wang, Y., Gao, Y., Su, J., Zhang, J., Xing, X., Zhou, C., Yao, K., An, Q., and Zhang, Y. (2018). H3K9 demethylase KDM4E is an epigenetic regulator for bovine embryonic development and a defective factor for nuclear reprogramming. *Development* **145**, dev158261.
- Lohmann, F., Loureiro, J., Su, H., Fang, Q., Lei, H., Lewis, T., Yang, Y., Labow, M., Li, E., Chen, T., and Kadam, S. (2010). KMT1E mediated H3K9 methylation is required for the maintenance of embryonic stem cells by repressing trophectoderm differentiation. *Stem Cells* **28**, 2011–212.
- Love, M.I., Huber, W., and Anders, S. (2014). Moderated estimation of fold change and dispersion for RNA-seq data with DESeq2. *Genome Biol.* **15**, 550.
- Lu, J.V., Weist, B.M., van Raam, B.J., Marro, B.S., Nguyen, L.V., Srinivas, P., Bell, B.D., Luhrs, K.A., Lane, T.E., Salvesen, G.S., and Walsh, C.M. (2011). Complementary roles of Fas-associated death domain (FADD) and receptor interacting protein kinase-3 (RIPK3) in T-cell homeostasis and antiviral immunity. *Proc. Natl. Acad. Sci. USA* **108**, 15312–15317.
- Macfarlan, T.S., Gifford, W.D., Agarwal, S., Driscoll, S., Lettieri, K., Wang, J., Andrews, S.E., Franco, L., Rosenfeld, M.G., Ren, B., and Pfaff, S.L. (2011). Endogenous retroviruses and neighboring genes are coordinately repressed by LSD1/KDM1A. *Genes Dev.* **25**, 594–607.
- Macfarlan, T.S., Gifford, W.D., Driscoll, S., Lettieri, K., Rowe, H.M., Bonanomi, D., Firth, A., Singer, O., Trono, D., and Pfaff, S.L. (2012). Embryonic stem cell potency fluctuates with endogenous retrovirus activity. *Nature* **487**, 57–63.
- Maksakova, I.A., Thompson, P.J., Goyal, P., Jones, S.J., Singh, P.B., Karimi, M.M., and Lorincz, M.C. (2013). Distinct roles of KAP1, HP1 and G9a/GLP in silencing of the two-cell-specific retrotransposon MERVL in mouse ES cells. *Epigenetics Chromatin* **6**, 15.
- Matoba, S., Liu, Y., Lu, F., Iwabuchi, K.A., Shen, L., Inoue, A., and Zhang, Y. (2014). Embryonic development following somatic cell nuclear transfer impeded by persisting histone methylation. *Cell* **159**, 884–895.
- Matsui, T., Leung, D., Miyashita, H., Maksakova, I.A., Miyachi, H., Kimura, H., Tachibana, M., Lorincz, M.C., and Shinkai, Y. (2010). Proviral silencing in embryonic stem cells requires the histone methyltransferase ESET. *Nature* **464**, 927–931.
- Nicetto, D., Donahue, G., Jain, T., Peng, T., Sidoli, S., Sheng, L., Montavon, T., Becker, J.S., Grindheim, J.M., Blahnik, K., et al. (2019). H3K9me3-heterochromatin loss at protein-coding genes enables developmental lineage specification. *Science* **363**, 294–297.
- Pedregosa, F., Varoquaux, G., Gramfort, A., Michel, V., Thirion, B., Grisel, O., Blondel, M., Prettenhofer, P., Weiss, R., Dubourg, V., et al. (2011). Scikit-learn: Machine Learning in Python. *JMLR* **12**, 2825–2830.
- Percharde, M., Lin, C.J., Yin, Y., Guan, J., Peixoto, G.A., Bulut-Karslioglu, A., Biechele, S., Huang, B., Shen, X., and Ramalho-Santos, M. (2018). A LINE1-Nucleolin Partnership Regulates Early Development and ESC Identity. *Cell* **174**, 391–405.
- Ramírez, F., Ryan, D.P., Grüning, B., Bhardwaj, V., Kilpert, F., Richter, A.S., Heyne, S., Dündar, F., and Manke, T. (2016). deepTools2: a next generation web server for deep-sequencing data analysis. *Nucleic Acids Res.* **44** (W1), W160–W165.
- Rodríguez-Terrones, D., Gaume, X., Ishiyuchi, T., Weiss, A., Kopp, A., Kruse, K., Penning, A., Vaquerizas, J.M., Brino, L., and Torres-Padilla, M.E. (2018). A molecular roadmap for the emergence of early-embryonic-like cells in culture. *Nat. Genet.* **50**, 106–119.
- Rowe, H.M., Jakobsson, J., Mesnard, D., Rougemont, J., Reynard, S., Aktas, T., Maillard, P.V., Layard-Liesching, H., Verp, S., Marquis, J., et al. (2010). KAP1 controls endogenous retroviruses in embryonic stem cells. *Nature* **463**, 237–240.
- Shan, B., Pan, H., Najafav, A., and Yuan, J. (2018). Necroptosis in development and diseases. *Genes Dev.* **32**, 327–340.
- Sharif, J., Endo, T.A., Nakayama, M., Karimi, M.M., Shimada, M., Katsuyama, K., Goyal, P., Brind'Amour, J., Sun, M.A., Sun, Z., et al. (2016). Activation of Endogenous Retroviruses in Dnm11(-/-) ESCs Involves Disruption of SETDB1-Mediated Repression by NP95 Binding to Hemimethylated DNA. *Cell Stem Cell* **19**, 81–94.
- Slee, E.A., Zhu, H., Chow, S.C., MacFarlane, M., Nicholson, D.W., and Cohen, G.M. (1996). Benzyloxycarbonyl-Val-Ala-Asp (OMe) fluoromethylketone (Z-VAD.FMK) inhibits apoptosis by blocking the processing of CPP32. *Biochem. J.* **315**, 21–24.
- Soufi, A., Donahue, G., and Zaret, K.S. (2012). Facilitators and impediments of the pluripotency reprogramming factors' initial engagement with the genome. *Cell* **151**, 994–1004.
- Spruijt, C.G., Gnerlich, F., Smits, A.H., Pfaffeneder, T., Jansen, P.W., Bauer, C., Münzel, M., Wagner, M., Müller, M., Khan, F., et al. (2013). Dynamic readers

- for 5-(hydroxy)methylcytosine and its oxidized derivatives. *Cell* 152, 1146–1159.
- Stancheva, I. (2005). Caught in conspiracy: cooperation between DNA methylation and histone H3K9 methylation in the establishment and maintenance of heterochromatin. *Biochem. Cell Biol.* 83, 385–395.
- Torrano, J., Al Emran, A., Hammerlindl, H., and Schaidler, H. (2019). Emerging roles of H3K9me3, SETDB1 and SETDB2 in therapy-induced cellular reprogramming. *Clin. Epigenetics* 11, 43.
- Tsunoda, Y., and McLaren, A. (1983). Effect of various procedures on the viability of mouse embryos containing half the normal number of blastomeres. *J. Reprod. Fertil.* 69, 315–322.
- Wang, H., An, W., Cao, R., Xia, L., Erdjument-Bromage, H., Chatton, B., Tempst, P., Roeder, R.G., and Zhang, Y. (2003). mAM facilitates conversion by ESET of dimethyl to trimethyl lysine 9 of histone H3 to cause transcriptional repression. *Mol. Cell* 12, 475–487.
- Wang, C., Liu, X., Gao, Y., Yang, L., Li, C., Liu, W., Chen, C., Kou, X., Zhao, Y., Chen, J., et al. (2018). Reprogramming of H3K9me3-dependent heterochromatin during mammalian embryo development. *Nat. Cell Biol.* 20, 620–631.
- Wegner, K.W., Saleh, D., and Degterev, A. (2017). Complex pathologic roles of RIPK1 and RIPK3: moving beyond necroptosis. *Trends Pharmacol. Sci.* 38, 202–225.
- Wei, J., Antony, J., Meng, F., MacLean, P., Rhind, R., Laible, G., and Oback, B. (2017). KDM4B-mediated reduction of H3K9me3 and H3K36me3 levels improves somatic cell reprogramming into pluripotency. *Sci. Rep.* 7, 7514.
- Weinlich, R., Oberst, A., Beere, H.M., and Green, D.R. (2017). Necroptosis in development, inflammation and disease. *Nat. Rev. Mol. Cell Biol.* 18, 127–136.
- Whiddon, J.L., Langford, A.T., Wong, C.J., Zhong, J.W., and Tapscott, S.J. (2017). Conservation and innovation in the DUX4-family gene network. *Nat. Genet.* 49, 935–940.
- Yan, Y.L., Zhang, C., Hao, J., Wang, X.L., Ming, J., Mi, L., Na, J., Hu, X., and Wang, Y. (2019). DPPA2/4 and SUMO E3 ligase PIAS4 oppositely regulate zygotic transcriptional program. *PLoS Biol.* 17, e3000324.
- Yang, L., Xia, L., Wu, D.Y., Wang, H., Chansky, H.A., Schubach, W.H., Hickstein, D.D., and Zhang, Y. (2002). Molecular cloning of ESET, a novel histone H3-specific methyltransferase that interacts with ERG transcription factor. *Oncogene* 21, 148–152.
- Ying, Q.L., Wray, J., Nichols, J., Batlle-Morera, L., Doble, B., Woodgett, J., Cohen, P., and Smith, A. (2008). The ground state of embryonic stem cell self-renewal. *Nature* 453, 519–523.
- Yuan, P., Han, J., Guo, G., Orlov, Y.L., Huss, M., Loh, Y.H., Yaw, L.P., Robson, P., Lim, B., and Ng, H.H. (2009). Eset partners with Oct4 to restrict extraembryonic trophoblast lineage potential in embryonic stem cells. *Genes Dev.* 23, 2507–2520.
- Zhang, Y., Liu, T., Meyer, C.A., Eeckhoute, J., Johnson, D.S., Bernstein, B.E., Nussbaum, C., Myers, R.M., Brown, M., Li, W., and Liu, X.S. (2008). Model-based analysis of ChIP-Seq (MACS). *Genome Biol.* 9, R137.
- Zhang, X., Smits, A.H., van Tilburg, G.B., Ovaa, H., Huber, W., and Vermeulen, M. (2018). Proteome-wide identification of ubiquitin interactions using UblA-MS. *Nat. Protoc.* 13, 530–550.

STAR★METHODS

KEY RESOURCES TABLE

REAGENT or RESOURCE	SOURCE	IDENTIFIER
Antibodies		
Rabbit polyclonal anti-SETDB1	GeneTex	Cat# GTX115305; RRID:AB_11176036
Rabbit polyclonal anti-HA	abcam	CAT# ab9110; RRID:AB_307019
Rabbit polyclonal anti-Nanog	BETHYL	Cat# A300-397A; RRID:AB_386108
Rabbit polyclonal anti-H3K9me3	abcam	Cat# ab8898; RRID:AB_306848
Rabbit polyclonal anti-H3K27me3	Millipore	Cat# 17-622; RRID:AB_916347
Rabbit polyclonal anti-GAPDH	Bioworld	Cat# AP2063; RRID:AB_2107445
IgG	abcam	Cat# ab37415; RRID:AB_2631996
Mouse polyclonal anti-RIPK1	BD	Cat# 610459; RRID:AB_397832
Rabbit polyclonal anti-RIPK3	Enzo	Cat#AD1-905-242-100; RRID:AB_2039527
Rabbit polyclonal anti-pRIPK1	CST	Cat#31122; RRID:AB_2799000
Rabbit polyclonal anti-pMLKL	CST	Cat#37333; RRID:AB_2799112
CASPASE8	proteintech	Cat#13423-1-AP; RRID:AB_2068463
Chemicals, Peptides, and Recombinant Proteins		
Leukemia Inhibitory Factor (LIF)	Millipore	Cat#ESGE107
CHIR99021	Sigma	Cat#SML1046-5MG
PD0325901	Sigma	Cat#PZ0162-5MG
FBS	GIBCO	Batch#10100147
DMEM-Dulbecco's Modified Eagle Medium, High Glucose	Hyclone	Cat#SH30022-2B
Knockout DMEM	GIBCO	Cat#10829018
GlutaMAX	GIBCO	Cat#35050079
Non-Essential Amino Acids Solution	GIBCO	Cat#11140076
β -Mercaptoethanol	GIBCO	Cat#21985-023
Sodium Pyruvate Solution	GIBCO	Cat#11360070
Penicillin-Streptomycin Solution	Hyclone	Cat#SV30010
DAPI	Sigma-Aldrich	Cat# D9542
Phosphate-Buffer Saline (PBS)	GIBCO	Cat#C14190500BT
Trypsin-EDTA (0.25%)	GIBCO	Cat#25200114
Trypsin-EDTA (0.05%)	GIBCO	Cat# 25300120
0.1% Gelatin Solution	Millipore	Cat#ES-006-B
Oligo-dT	TaKaRa	Cat#D511
RRI	TaKaRa	Cat#D2313A
SsoAdvanced Universal SYBR Green Supermix	Bio-Rad	Cat#172-5274
DNase/RNase Free Deionized Water	TIANGEN	Cat#RT121
RIP inhibitor Necrostatin-1(Nec-1)	Selleck	Cat#C0037
Caspase inhibitor Z-VAD-FMK	Selleck	Cat#S7023
Lipofectamine RNAiMAX Transfection Reagent	Invitrogen	Cat#13778150
4-hydroxytamoxifen	Selleck	Cat#S7827
Hygromycin	Selleck	Cat#S2908
Puromycin	GIBCO	Cat#A1113802
Critical Commercial Assays		
ChamQ™ SYBR® QPCR Master Mix	Vazyme Biotech	Q311
VAHTS™ mRNA-seq V3 Library Prep Kit for Illumina	Vazyme Biotech	NR611
TruePrep™ DNA Library Prep Kit V2 for Illumina	Vazyme Biotech	TD-501-503

(Continued on next page)

Continued		
REAGENT or RESOURCE	SOURCE	IDENTIFIER
MinElute Reaction Clean up Kit	QIAGEN	28006
NextSeq500 High output 150 cycles	Illumina	FC-404-2002
AMPure XP beads	BEECKMAN COULTER	Cat#A63882
Quant-IT™ Picogreen dsDNA Assay kit	Life Technologies	CAT#P11496
NextSeq500 Mid output 150 cycles	Illumina	FC-404-2001
Deposited Data		
RNA-seq Data	This paper	PRJNA544540
ChIP-seq Data	This paper	PRJNA544540
Experimental Models: Cell Lines		
OG2 Mouse Embryonic Stem cells: CBA/CaJ x	This paper	N/A
MERVL::TdTomato reporter mouse embryonic stem cells	A gift from Prof. Yangming Wang laboratory	N/A
Setdb1 CKO mouse embryonic stem cells	This paper	N/A
Experimental Models: Organisms/Strains		
OG2 mice	The Jackson Laboratory	Mouse strain datasheet: 004654
129 mice	Beijing Vital River Laboratory Animal Technology	Stock No.: 217
CD-1 mice	Beijing Vital River Laboratory Animal Technology	Stock No.: 201
Oligonucleotides		
Oligonucleotides are summarized in Table S4	This paper	N/A
Recombinant DNA		
PB-TRE-Ripk1-HA	This paper	N/A
pRenti-Setdb1	This paper	N/A
pB-TRE-HA-Setdb1	This paper	N/A
pLKO.1-shRipk3	This paper	N/A
pLKO.1-shCaspase8	This paper	N/A
Rosa26 MERVL::TdTomato donor	A gift from Prof. Yue Huang laboratory	N/A
Software and Algorithms		
FlowJo	Ashland	https://www.flowjo.com/solutions/flowjo/downloads
GraphPad Prism 5	GraphPad Software	https://www.graphpad.com/support/faqid/1952/
ZEN 2009	Zeiss	https://www.zeiss.com/microscopy/int/downloads.html?vaURL=www.zeiss.com/microscopy/int/downloads/zen.html
Bio-RAD CFX Manager	BIO-RAD	http://www.bio-rad.com/en-us/product/cfx-manager-software?tab=Download
Beacon Designer	PREMIER Biosoft	http://www.premierbiosoft.com/molecular_beacons/
Illustrator	Adobe System Software Ireland	http://www.adobe.com/cn/products/cs6/illustrator.html
ImageJ	NIH, USA	https://imagej.nih.gov/ij
mfuzz	R package (Matthias Futschik)	http://www.bioconductor.org/packages/release/bioc/html/Mfuzz.html
maSig	R package (Ana Conesa, Maria Jose Nueda)	https://bioconductor.org/packages/release/bioc/html/maSigPro.html
GOseq	R package (Matthew Young)	http://www.bioconductor.org/packages/release/bioc/html/goseq.html

(Continued on next page)

Continued		
REAGENT or RESOURCE	SOURCE	IDENTIFIER
Bowtie2	Langmead and Salzberg, 2012	http://bowtie-bio.sourceforge.net/bowtie2/manual.shtml
MACS2	Zhang et al., 2008	https://pypi.org/project/MACS2/
Dfilter	Kumar et al., 2013	https://reggenlab.github.io/DFilter/
Deeptools	Ramírez et al., 2016	https://deeptools.readthedocs.io/en/develop/
Homer	Heinz et al., 2010	http://homer.ucsd.edu/homer/
DESeq2	Love et al., 2014	R package DESeq2
scikit-learn	Pedregosa et al., 2011	https://scikit-learn.org/stable/index.html
matplotlib	Hunter, 2007	https://matplotlib.org/index.html
seaborn	Michael Waskom	http://seaborn.pydata.org/index.html
Accuri C6 Plus	BD biosciences	http://www.bdbiosciences.com/us/instruments/research/cell-analyzers/bd-accuri/m/1294932/overview
Photoshop	Adobe System Software Ireland	http://www.adobe.com/cn/products/cs6/photoshop.html
Other		
DNA methylation data	Habibi et al., 2013	GSE41923
2C and ZGA data	Li et al., 2017b	GSE44183
Setdb1 CKO data	Karimi et al., 2011	GSE29413
Setdb1 KD data	Yuan et al., 2009	GSE17642

LEAD CONTACT AND MATERIALS AVAILABILITY

Further information and requests for resources and reagents may be directed to the Lead Contact, Jiekai Chen (chen_jiekai@gibh.ac.cn)

EXPERIMENTAL MODEL AND SUBJECT DETAILS

Mouse Strains

OG2 mice had a CBA/CaJ × C57BL/6J background (Mouse strain datasheet: 004654). CD-1 mice were used as embryo donors and the pseudopregnant recipients for blastocyst injection. CD-1 (Stock No.: 201) and 129 (Stock No.: 217) mice were obtained from Beijing Vital River Laboratory Animal Technology Co., Ltd. Animal experiments were performed in accordance with the Guide of the Care and Use of Laboratory Animals by the National Research Council and approved by (GIBH) Institutional Animal Care and Use Committee.

Cell Lines and Cell Culture Condition

OG2 mouse embryonic stem cells were derived from 3.5 d.p.c ICM from 129 female mice crossing male OG2 mice. MERVL::tdTomato reporter ESC line is a gift Prof. Yangming Wang. ESCs were cultured independent of feeders in two types of media: 1000U/mL LIF in DMEM containing 15% fetal calf serum (SL); 1000U/mL LIF in serum-free N2B27 medium supplemented with MEK inhibitor PD0325901 (1 μM) and GSK3 inhibitor CHIR99021 (3 μM), known as 2i (2iL) (Ying et al., 2008).

METHOD DETAILS

Generation of Setdb1 Conditional Knockout OG2 mES Cell

In brief, two loxP sites were inserted into endogenous Setdb1 locus (Setdb1 ENSMUSG0000001569 7; SET domain, bifurcated 1, MGI: 1934229) flanking exon16 with CRISPR Cas9 and donor plasmid. Then we introduce PGK-CreERT into another allele replacing 16exon of Setdb1 by homologous recombination. The cells were selected with Puromycin (1 μg/ml) for 3 days and conducted genotype identification with genome PCR and western blot. Finally, we can get Setdb1 knockout OG2 mESCs by adding 0.5 μM 4-hydroxytamoxifen (4OHT).

Construction of Reporter Cell Lines

MERVL::tdTomato reporter ESC line for Figure 3A is reported in previous study (Yan et al., 2019). To generate Rosa26 loci knock-in 2C::tdTomato reporter cell line on Setdb1-CKO ESCs, the Rosa26 targeting MERVL-LTR-tdTomato reporter (a generous gift from Dr.

Yue Huang, Chinese Academy of Medical Sciences) was linearized and transfected into ESCs by electroporation. The cells were then selected with Hygromycin (200 $\mu\text{g}/\text{ml}$) for 5 days. Colonies containing tdTomato-positive cells were subsequently picked and expanded. All cell lines were kept under constant drug selection with Hygromycin. Mycoplasma detection tests were conducted routinely to ensure mycoplasma-free conditions throughout the study.

Gene Knockdown Assay

siRNAs were suspend-transfected twice at Day0 and Day2 using Lipofectamine RNAiMAX Transfection Reagent (13778150, Invitrogen) according to the manufacturer's instructions. shRNA were constructed into pLKO.1 constructor (Table S4). Lentivirus was prepared by transfecting 293T cells, as previously described (Castro-Diaz et al., 2014; Rowe et al., 2010). Briefly, The virus was harvested 48 h after transfection and pre-infected 2 days (for 8h with twice) to ensure its knockdown efficiency before 4OHT treatment.

Western Blot

Western blots were performed using typical laboratory procedures with the following antibodies: anti-NANOG (A300-397A, Bethyl), anti-SETDB1 (GTX115305, GeneTex), anti-GAPDH (MAB374, Millipore), anti-RIPK1 (17519-1-AP, Proteintech), anti-RIPK3 (17563-1-AP, Proteintech), anti-pMLKL (37333, CST), and anti-pRIPK1 (31122, CST). Briefly, cells were lysed on ice in SDS buffer (62.5 mM Tris-HCl (pH 6.8 at 25°C). Whole-cell extracts were resolved by 10% or 12% SDS-PAGE, transferred to PVDF membranes and probed with corresponding antibodies according to the manufacturer's recommendations (Cell Signaling Technology).

Immunofluorescence Staining

Cells growing on a confocal dish (801002, NEST) were fixed in 4% paraformaldehyde for 30 min, washed with PBS three times and permeabilized with 0.2% Triton X-100 and 3% BSA for 30min at room temperature. Then the cells were incubated with anti-NANOG (A300-397A, Bethyl) for 2 h. Following PBS washes, the secondary antibody (A11011, Invitrogen) was applied for 1h and subsequently, DAPI for 2 min. Finally, the coverslips were mounted on slides for observation.

Cell Survival Assay

Cell survival assay was performed using the Cell Counting Kit-8 Assay kit according to the manufacturer's instructions (C0037, Beyotime). ESCs underwent pre-treatment with 50 μM Caspase inhibitor Z-VAD-FMK (S7023, Selleck) and 30 μM RIP inhibitor Necrostatin-1 (S8037, Selleck) along with 0.5 μM 4OHT for 2 days, followed by re-plating for 4 days.

Flow Cytometry

Cells were digested by 0.05% trypsin and re-suspended with PBS with 2% FBS (FACS buffer) for direct detection. The suspension was filtered with a strainer and analyzed using Fortessa cytometer (BD Biosciences, San Jose, CA). The GFP fluorescence intensity were detected in the FITC channel, and mCherry in PE channel. Data were analyzed using FlowJo software (FlowJo, LLC, Ashland, OR, USA).

Co-immunoprecipitation (Co-IP)

RIP1-HA overexpression Setdb1 CKO mES cells were collected with 1×10^7 cells per tube. The cells were re-suspended in 1ml Lysis buffer (150 mM NaCl, 50 mM Tris-HCl pH 7.4, 2 mM EDTA, 1% NP-40, and protease inhibitors) and rotated 30min at 4°C. Cell lysate was collected by centrifugation (10,000 g, 10min at 4°C) and incubated with 20ul Anti-HA Magnetic Beads (88837, Sigma) for 30 minutes at room temperature. Beads were washed with lysis buffer for 5 times (10 min each time) and boiled in SDS buffer for 10 min to elute the protein complex.

Immunoprecipitation (IP)-MS

RIP1 HA-tag Immunoprecipitation and On-bead Digestion. Whole cell extracts of mES cells with Ripk1-HA overexpression were prepared using lysis buffer (50 mM Tris pH 8.0, 150 mM NaCl, 10% Glycerol, 0.5% NP40) with fresh added Complete Protease inhibitors (Sigma, 1187358001). Cells were incubated for 2h at 4°C with rotation. Soluble cell lysates were collected by centrifugation (12,000 g, 15min at 4°C). 1 mg of cell lysates were incubated with either HA antibody or matched IgG overnight at 4°C with rotation. Combined Protein A/G magnetic beads (Bio-rad, 1614833) were added for another 1.5 h. Beads were then washed 3 times with wash cell lysis buffer and 1 time with PBS. After completely removal of PBS, immunoprecipitated proteins were digested using on-bead digestion protocol as described before (Spruijt et al., 2013). Briefly, beads were incubated with 100 μL of elution buffer (2 M urea, 10 mM DTT and 100 mM Tris pH 8.5) for 20 min. Then, iodoacetamide (Sigma, I1149) was added to a final concentration of 50 mM for 10min away from light, following with 250 ng of trypsin (Promega, V5280) partially digestion for 2 h. After incubation, the supernatant was collected in a separate tube. The beads were then incubated with 100 μL of elution buffer for another 5min, and the supernatant was collected in the same tube. All these steps were performed at RT in a thermoshaker at 1500 rpm. Combined elutes were digested with 100 ng of trypsin overnight at RT. Finally, tryptic peptides were acidified to pH < 2 by adding 10 mL of 10% TFA (Sigma, 1002641000) and desalted using C18 Stagetips (Sigma, 66883-U) prior to MS analyses.

Mass Spectrometry Analysis

RIP Tryptic peptides were separated using a total 140 min of data collection (100 min of 2% to 22%, 20 min 22% to 28% and 12 min of 28% to 36% gradient of acetonitrile (Thermo, 51101) for peptide separation, following with two steps washes: 2 min of 36% to 100% and 6 min of 100% acetonitrile) with an Easy-nLC 1200 connected online to a Fusion Lumos mass spectrometer (Thermo). Scans were collected in data-dependent top-speed mode with dynamic exclusion at 90 s. Raw data were analyzed using MaxQuant version 1.6.0.1 search against Mouse Fasta database, with label free quantification and match between runs functions enabled. The output protein list was analyzed and visualized using DEP package as described before (Zhang et al., 2018).

Native ChIP

Native ChIP protocol was performed as previously described (Hasson et al., 2013). One million mES cells were collected and washed with PBS, then centrifuged and resuspended in 0.25ml of Buffer1 (0.32M Sucrose, 60mM KCl, 15mM NaCl, 5mM MgCl₂, 0.1mM EGTA, 15mM Tris-HCl pH7.5, 0.5mM DTT, 0.1mM PMSF, 1:1000 protease inhibitor cocktail (Sigma-Aldrich)), along with 0.25ml of Buffer1+0.1%IGEPAL. The resulting 0.5ml of nuclei were layered on top of 1ml of Buffer3 (Same as Buffer1, but with 1.2M Sucrose) and centrifuged at 10,000 g for 20 min at 4°C unbraked. Nuclei were resuspended in Buffer A (0.34M sucrose, 15mM HEPES, pH7.4, 15mM NaCl, 60mM KCl, 4mM MgCl₂, 1mM DTT, 0.1mM PMSF, 1:1000 protease inhibitor cocktail (Sigma-Aldrich)) and digested for 20 min at 37°C with MNase(Sigma) in Buffer A supplemented with 3mM CaCl₂. The reaction was stopped with 5mM EGTA, centrifuged at 13,500 g for 10 min, and chromatin resuspended in (10mM EDTA, pH8.0, 1mM PMSF, 1:1000 protease inhibitor cocktail) and rotated at 4°C for 2-4h. The mixture was adjusted to 500mM NaCl, allowing rotation for another 45 min and then centrifuged at 13,500 g for 10 min. Chromatin supernatant was diluted to 100ng/μl with buffer B (20mM Tris, pH8.0, 5mM EDTA, 500mM NaCl, 0.2% Tween20) and incubated for 20 min at 4°C with 60 μL protein G + protein A beads (GE Healthcare). Antibodies were added and rotated overnight at 4°C. The beads were washed three times with Buffer B, and once with Buffer B without Tween 20. The DNA was eluted with 300 μL of elution buffer (20mM Tris (pH7.5), 20mM EDTA, 0.5% SDS, 500ug/ml Proteinase K) and incubated for 4h at 56°C. The resulting samples were purified with QIAGEN MinElute columns, according to the manufacturer's instructions. Antibodies used: anti-H3K9me3 (5 μg; ab8898, abcam), anti-H3K27me3 (5 μg, 17-622, Millipore).

ChIP-Seq

Setdb1 ChIP was performed as described previously (Chen et al., 2013). ESCs were fixed with 1% formaldehyde for 12min and the reaction was quenched by 0.125M glycine. Cells were then washed with PBS for three times. Cells were lysed in ChIP buffer (1% SDS, 50 mM Tris-HCl, pH 8.0, 10 mM EDTA, and protease inhibitor cocktail) for 10 min at 4°C. The DNA was fragmented to 200-500bp by sonication and centrifuged at 12,000 g for 2min. The supernatant was diluted with ChIP IP buffer (50 mM Tris-HCl, pH 8.0, 150 mM NaCl and protease inhibitor cocktail). Immunoprecipitation was performed with 5 μg rabbit anti-Setdb1 antibody (GTX115305, GeneTex) coupled to protein A/G overnight at 4°C. Beads were washed, eluted, and reverse cross-linked. DNA was purified using the MinElute Reaction Clean up Kit (QIAGEN). The ChIP DNA library for NextSeq 500 sequencing was constructed with VAHTS Turbo DNA Library Prep Kit for Illumina (Vazyme Biotech) according to the manufacturer's instructions. AMPure XP beads were used for purification steps. The library was quantified with VAHTS Library Quantification Kit for Illumina (Vazyme Biotech) and sequenced on an Illumina NextSeq 500 v2 with 50bp paired-end reads. Annoroad Gene Technology company (Beijing, China) performed the DNA sequencing.

qRT-PCR and RNA-Seq

Total RNA was extracted with a TRIzol-based protocol. For quantitative PCR, cDNA was synthesized with ReverTra Ace (Toyobo) and oligo-dT (Takara), and then analyzed by qPCR with Premix Ex Taq (Takara). VAHTS mRNA-seq V3 Library Prep Kit for Illumina (NR611, Vazyme) was used for library constructions and sequencing done with NextSeq500 Mid output 150 cycles (FC-404-2001, Illumina) for RNA-seq. The qPCR primers can be found in Table S4. Annoroad Gene Technology company (Beijing, China) performed the DNA sequencing.

RNA-Seq, ChIP-Seq Analysis

RNA-seq clean reads were mapped to mouse transcript annotation of Gencode vM15 version on mm10 genome using RSEM (Collier et al., 2017). We chose Trans Per Million (TPM) value for the normalization and evaluation of gene expression levels. Meanwhile, ChIP-seq clean reads were mapped to mm10 genome using Bowtie2 package (Langmead and Salzberg, 2012). Then we applied MACS2 (Zhang et al., 2008) and Dfilter (Kumar et al., 2013) to call the enriched peaks. Deeptools (Ramírez et al., 2016) and Homer (Heinz et al., 2010) were applied to calculate the ChIP-seq peak profiles of nearby genes. Data analysis and visualizations were performed in R environment.

Gene Set Enrichment Analysis (GSEA) was used to determine whether the Setdb1-KO upregulated genes were enriched for genes that are specifically expressed at the 2-cell stage or during ZGA as described previously (Li et al., 2017b). We used the following published datasets for analysis: DNA methylation (GSE41923, Habibi et al., 2013).

QUANTIFICATION AND STATISTICAL ANALYSIS

Data are presented as mean \pm s.e.m. or mean \pm s.d. as indicated in the figure legends. Unpaired two-tailed Student's t test, Two-way AVOVA with Sidak's multiple comparisons test were used to assess statistical significance. The p value, t-ratio were calculated with the Prism 6 software. A p value < 0.05 was considered as statistically, *p < 0.05 , **p < 0.01 , ***p < 0.001 . No statistical method was used to predetermine sample size.

DATA AND CODE AVAILABILITY

Accession Numbers

A BioProject accession number (PRJNA544540) has been assigned to the sequencing data of this manuscript. Other published datasets can be found in "Other" section of [Key Resources Table](#).